Modeling action potential reversals in tunicate hearts

John W. Cain* and Luran He
Department of Mathematics, Harvard University, Cambridge, Massachusetts 02138, USA

Lindsay Waldrop
Department of Biological Sciences, Chapman University, Orange, California 92866, USA

(Received 7 August 2020; revised 12 November 2020; accepted 30 November 2020; published 23 December 2020)

Tunicates are small invertebrates which possess a unique ability to reverse flow in their hearts. Scientists have debated various theories regarding how and why flow reversals occur. Here we explore the electrophysiological basis for reversals by simulating action potential propagation in an idealized model of the tubelike tunicate heart. Using asymptotic formulas for action potential duration and conduction velocity, we propose tunicate-specific parameters for a two-current ionic model of the action potential. Then, using a kinematic model, we derive analytical criteria for reversals to occur. These criteria inform subsequent numerical simulations of action potential propagation in a fiber paced at both ends. In particular, we explore the role that variability of pacemaker firing rates plays in generating reversals, and we identify various favorable conditions for triggering retrograde propagation. Our analytical framework extends to other species; for instance, it can be used to model competition between the sinoatrial node and abnormal ectopic foci in human heart tissue.

DOI: 10.1103/PhysRevE.102.062421

I. INTRODUCTION

Tunicates (Chordata:Urochordata) are marine invertebrate animals named for their tuniclike outer coverings. They are our closest living invertebrate relatives [1] and serve as a model for development of vertebrate chambered hearts [2–4]. Species such as *Ciona intestinalis* and *Ciona savignyi*, commonly known as "sea squirts," may have body lengths of 10 cm or more, and their tubular hearts have lengths on the order of 3 cm. The tunicate heart consists of a tube of contractile myocardium surrounded by an outer, stiff, noncontractile pericardium [5]. The myocardium is a single layer of myocardial cells wrapped around an inner lumen and fused at the raphe, which extends longitudinally along the heart [5,6]. The myocardium contracts to reduce the diameter of the inner lumen and drive fluid longitudinally through the lumen.

Tunicates are peculiar organisms in that their hearts occasionally reverse the direction of blood flow. Often, time intervals between consecutive reversals are on the order of minutes. Some scholars [7] have speculated that heart reversals help tunicates more effectively distribute oxygen and nutrients throughout their entire bodies. This remains one of the most accepted ideas of *why* reversals may occur. Here we explore mechanisms for *how* reversals may occur and identify conditions favorable for generating reversals.

Among the many early theories regarding mechanisms for reversals, just over half a century ago, two dominant ideas emerged. Haywood and Moon [8,9] advocated a then-century-old "back-pressure theory" that reversals occur due to a congestion-induced buildup of pressure. Subsequent experiments of Krijgsman [10] showed that reversals still occur in isolated hearts, suggesting that blood pressure is not necessary for reversals. Krijgsman's study focused on the role of fatigue of the small clusters of specialized pacemaker cells located at opposite ends of the heart. He argued that reversals may occur due to "pacemaker fatigue," an increase in the excitation threshold for cells over the time course of a train of electrical stimuli. If pacemaker A fires more slowly than pacemaker B, then pacemaker B may "overdrive" pacemaker A, establishing sustained unidirectional propagation from B toward A. Pacemaker slowdown is one of the reversal mechanisms that we explore below; we also consider the role of stochastic variability in the interstimulus intervals of both pacemakers.

In this article, we propose a mathematical model for reversal of propagation in tunicate hearts, and we derive simple, analytical criteria for reversals to occur. We adopt a two-current model [11] of cardiac action potentials (Sec. II B), treating the tubular tunicate heart as a one-dimensional excitable medium paced at both ends. Highly accurate asymptotic approximations of action potential duration (APD) and conduction velocity (CV) are readily available for the two-current model, enabling us to predict the locations of wavefronts and wavebacks of each propagating action potential (AP). Tracking wavefronts and wavebacks is essential in the present context, as we must detect whether the heart exhibits sustained unidirectional propagation, intermittent reversals, repeated collisions of APs propagating in opposite directions, or some combination of all of these responses. The ability to observe reversals hinges on an appropriate balance among (i) the length of the heart, (ii) the firing rates of the pacemakers at both ends of the heart, and (iii) the APD and CV of the propagating APs. The fully kinematic model of wave propagation presented in Sec. II D gives rise to

*jcain2@math.harvard.edu

 ©2020 American Physical Society

analytical criteria for reversal of propagation (Sec. II E). A similar approach has been used previously [12] for the purpose of predicting AP propagation failure at a distance from a single pacing site; here, however, there are two pacing sites.

In Sec. III, we illustrate our model's ability to exhibit reversals in simulated tunicate hearts, comparing our simulated and experimentally observed reversals. Combining our own experimental observations with previously published data [13,14], the asymptotic formulas for APD and CV allow us to estimate tunicate-specific model parameters (Sec. III A). With the model parameters suitably tuned, we demonstrate reversals generated via two different mechanisms: Gradual variability of pacemaker firing rates and stochastic variability of interstimulus intervals of the two pacemakers with the same mean firing rate (Sec. III B). While it is certainly noteworthy that stochastic variability alone can elicit a reversal even if the mean interstimulus intervals of the two pacemakers are identical, our simulations of gradual pacemaker variability exhibit dynamical behavior far more reminiscent of experimental observations. Through additional numerical simulations, we demonstrate excellent quantitative agreement between the analytical criteria for reversals put forth in Sec. II E and the results of numerical simulations with two-current, PDE-based model. Section III C surveys our general observations regarding favorable conditions for generating reversals.

We believe that our results are interesting beyond the context of tunicate heart phenomena. In human hearts, the native pacemaker cells in the sinus node drive the normal contraction of heart muscle. When ectopic automaticity foci exist within the tissue, they may compete with the sinus node for control of rhythm. The mechanisms and modeling framework described here could be of importance in understanding mode transitions between competing automaticity foci in many organisms.

II. METHODS AND MATHEMATICAL MODELING

A. Experimental observation of reversals

Adult solitary tunicates (*Ciona savignyi* Herdman, 1882) were acquired from the University of California, Santa Barbara, Ciona Stock Center via overnight shipment. These animals were kept in a recirculating seawater system at 15°C in a 12-h light-dark cycle maintained with artificial seawater (Instant Ocean, Spectrum Brands, Madison, WI) of salinity 30–34 parts per thousand (ppt).

Adult tunicates were spawned using a dark-box technique to collect gametes, which were then combined in ultrafiltered seawater (Instant Ocean) at 32 ppt. Fertilized eggs were kept in Petri dishes at room temperature overnight to speed development, and then swimming larvae were transferred to clean, ultrafiltered seawater via pipette and floated in the recirculating tank held at 15°C. Twenty-four hours after fertilization, larvae settled on the surface of water to begin metamorphosis. These larvae were transferred to sterilized glass slides by dipping each slide into the surface of the water. Slides were then hung with larvae on the underside of the slide in the main recirculating tank and observed every second day.

Juvenile tunicates were observed using a Leica (Wetzlar, Germany) M165FC stereo dissecting scope using a dark field by placing the glass slide in a Petri dish containing filtered seawater. Videos were taken using Celestron SKYRIS 132C CMOS (Celestron, Torrance, CA) camera at 60 fps at 40× magnification. One such video is provided among the supplemental materials [15]. Examples of reversals occur at times 00:10, 02:20, and 02:50. A detailed discussion of the behaviors shown in the video appears in Sec. IV below.

B. Two-current ionic model

Readers seeking a more detailed overview of tunicate heart physiology and an experimentally informed electromechanical model of contraction are encouraged to read the article of Waldrop and Miller [16]. For our purpose of simulating mode competition between two pacemakers, it is not necessary to use a detailed cell membrane model accounting for how various ions are transported, exchanged, sequestered, etc. We modeled the tubular tunicate heart as a one-dimensional fiber of total length L and used the two-current model of Mitchell and Schaeffer [11] to simulate cardiac action potential propagation. The Mitchell-Schaeffer model is an attractive choice because previous studies [11,17,18] have reported highly accurate asymptotic approximations expressing both speed and duration of action potentials as functions of the model parameters (see next subsection). Those formulas guide our selection of parameters so as to observe reversals of propagation direction.

The two-current model equations are given by

$$\frac{\partial v}{\partial t} = \kappa \frac{\partial^2 v}{\partial x^2} + \frac{h}{\tau_{\text{in}}} v^2 (1 - v) - \frac{v}{\tau_{\text{out}}}, \tag{1}$$

$$\frac{\partial h}{\partial t} = \begin{cases} \dfrac{1 - h}{\tau_{\text{open}}} & \text{if } v \leqslant v_{\text{crit}} \\ -\dfrac{h}{\tau_{\text{close}}} & \text{if } v > v_{\text{crit}} \end{cases}, \tag{2}$$

on the spatial domain $0 < x < L$. The dynamic variables $v = v(x,t)$ and $h = h(x,t)$ are scaled to vary between 0 and 1, and they represent transmembrane voltage and an inactivation gate, respectively. Position x along the fiber and time t are measured in centimeters and milliseconds, respectively, unless otherwise noted. Regarding other notation within the model equations, κ is a diffusion coefficient, and τ_{in}, τ_{out}, τ_{open}, and τ_{close} are time constants associated with different phases of the action potential. The constant v_{crit} determines the threshold voltage above which h decays exponentially [shutting off the "inward current" term in (1)] and below which $(1 - h)$ decays exponentially. Homogeneous, no-flux boundary conditions $v_x(0,t) = v_x(L,t) = 0$ are imposed at both ends of the fiber. Stimuli are applied impulsively, instantaneously increasing v by 0.5 among all cells within 0.05 centimeters of an end of the fiber. None of the results reported below were affected when we repeated the simulations using a constant current (1 ms duration) to activate cells within 0.05 cm of the ends of the fiber.

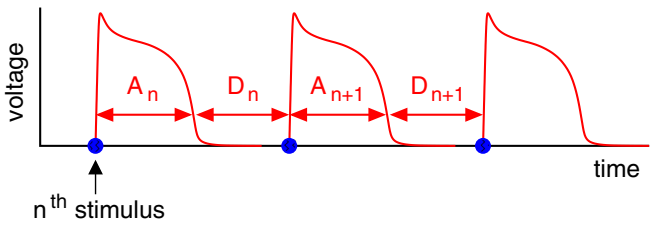

FIG. 1. Schematic action potentials. Bold dots indicate stimuli.

C. Restitution of action potential duration and conduction velocity

Repeated electrical stimulation of a cell, or *pacing*, elicits a sequence of action potentials. *Action potential duration* (APD) is defined as the amount of time for which v remains above some threshold, and for the Mitchell-Schaeffer model it is convenient to use v_{crit} as that threshold. The *diastolic interval* (DI) is defined as the amount of time over which $v \leqslant v_{\text{crit}}$ between consecutive action potentials. We will denote by A_n the APD following the nth stimulus which succeeds [19] in eliciting an action potential, and D_n will denote the subsequent DI (see Fig. 1). Action potentials propagate spatially, due to gap junctional coupling of neighboring cells. *Conduction velocity* (CV) refers to the speed with which action potentials propagate through tissue. By *restitution* of APD (or CV), we mean the dependence of APD (or CV) on the (local) DI. Typically, longer DI (i.e., more rest for the cells) leads to longer APD and faster CV, at least up to some plateau.

The simplicity of the two-current model equations (1) and (2) allows one to derive accurate asymptotic approximations for restitution of APD and CV. Within physiological parameter regimes, the time constants are well separated in that

$$\tau_{\text{in}} \ll \tau_{\text{out}} \ll \tau_{\text{open}}, \tau_{\text{close}}.$$

Now let $h_{\text{min}} = 4\tau_{\text{in}}/\tau_{\text{out}}$ and $\epsilon = \tau_{\text{out}}/\tau_{\text{close}}$, and define

$$h(D_n) = 1 - (1 - h_{\text{min}})e^{-D_n/\tau_{\text{open}}}.$$

Then using singular perturbation theory, one may show that

$$A_{n+1} \sim f(D_n) = \tau_{\text{close}} \ln\left[\frac{h(D_n)}{h_{\text{min}}}\right] + \zeta\,\tau_{\text{close}}\epsilon^{2/3}\left[\frac{1 - e^{-D_n/\tau_{\text{open}}}}{h(D_n)}\right], \quad (3)$$

where $\zeta = 2.33811\ldots$ is a root of the Airy function $\text{Ai}(-x)$; see Ref. [17] for details. A similar formula expressing CV as a function of DI may be derived by seeking periodic traveling wavetrain solutions of (1) and (2). If

$$V_{\pm}(D_n) = \frac{1}{2}\left[1 \pm \sqrt{1 - \frac{h_{\text{min}}}{h(D_n)}}\right],$$

then in leading-order asymptotics CV is approximated by

$$c(D_n) = \left[\frac{V_+(D_n)}{2} - V_-(D_n)\right]\sqrt{\frac{2\kappa h(D_n)}{\tau_{\text{in}}}}. \quad (4)$$

For details, refer to the Appendix of Ref. [18]. One caveat: Formulas (3) and (4) cannot be applied for DI so small that eliciting an action potential is impossible, i.e., for which the fiber has not recovered its excitability. In fact, for very small DI, Eq. (4) may return (unphysiological) negative values.

Importantly, formulas (3) and (4) explain how the speed and duration of action potentials are influenced by the diffusion constant κ and the four time constants associated with the phases of the action potential.

D. Kinematic model

In order to explain the reversal phenomenon, we recall a *kinematic* model of action potential propagation, using information encapsulated by the restitution functions (3) and (4). Figure 2(a) is a color-coded space-time plot of action potentials propagating left-to-right in a one-dimensional fiber, with stimuli repeatedly applied at the $x = 0$ end. Figure 2(b) indicates the progress of wavefronts (solid curves) and wavebacks (dashed curves) of the propagating action potentials. Let $\phi_n(x)$ and $\beta_n(x)$ denote the times at which the nth wavefront and waveback (respectively) arrive at position x along the fiber. If $A_n(x)$ and $D_n(x)$ indicate APD and DI at position x, then observe from the figure that

$$A_n(x) + D_n(x) = \phi_{n+1}(x) - \phi_n(x).$$

Applying the APD restitution function (3) locally [20] at each position x, we obtain

$$f(D_{n-1}(x)) + D_n(x) = \phi_{n+1}(x) - \phi_n(x).$$

Differentiating with respect to x and using the CV restitution function in Eq. (4) yields

$$\frac{d}{dx}[f(D_{n-1}(x)) + D_n(x)] = \frac{1}{c(D_n(x))} - \frac{1}{c(D_{n-1}(x))}. \quad (5)$$

Given a sequence of stimulus times at the $x = 0$ boundary together with an initial profile of DI values, $D_0(x)$, one may solve the sequence of differential equations (5) recursively. Combining the recursively obtained formulas for $D_n(x)$ with the restitution relationship $A_n(x) = f(D_{n-1}(x))$, one may generate Fig. 2(b) from a purely kinematic model.

Although APD and CV restitution functions may have nonmonotone dependence on DI, it is often the case that both f and c are increasing functions which plateau in the limit of large DI. For instance, APD restitution curves are commonly fit by functions of the form $f(D_n) = \alpha - \beta\exp(-D_n/\tau)$ for constants α, β, and τ (see Ref. [21]). If f is monotone increasing and a cell is paced with appropriately large period B, then there is a unique DI (call it D^*) for which $D^* + f(D^*) = B$. Indeed, provided that pacing is not too rapid (i.e., B is not too small) the generic steady-state behavior is a one-to-one response in which each DI equals D^* and each APD equals $f(D^*)$.

E. Conditions for reversal of propagation

Using the kinematic model in the previous subsection, let us derive criteria for the sudden reversal of left-to-right unidirectional propagation, assuming that the proximal ($x = 0$) pacemaker fires periodically with period B. The idea is that if a stimulus is applied at the distal ($x = L$) pacemaker within some "vulnerable time window," retrograde propagation will ensue. Depending on timing related issues that we shall explain, the right-to-left propagating action potential may either

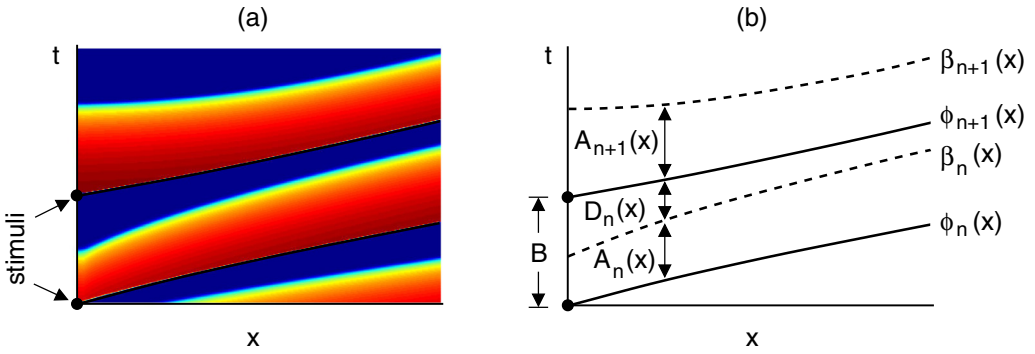

FIG. 2. (a) Color map of $v(x,t)$ obtained via numerical solution of Eqs. (1) and (2) for some choice of parameters and initial data. Blue (dark) regions indicate that v is close to the resting potential, while red and yellow (brighter) regions indicate elevated v. Stimuli at the left boundary are indicated and induce left-to-right propagation. (b) Schematic space-time plot of the wavefronts (solid curves) and wavebacks (dashed curves) in panel (a).

(i) traverse the entire fiber uninterrupted or (ii) collide with a subsequent left-to-right action potential generated by the proximal pacemaker.

Suppose that a fiber has achieved (approximate) steady state in which action potentials propagate left-to-right, with spatially uniform APD and CV. In such a case, a space-time plot of wavefronts and wavebacks [as in Fig. 2(b)] would appear as a collection of parallel lines, with $D_n(x) = D^*$ and $A_n(x) = f(D^*)$ for each n and for $0 \leqslant x \leqslant L$. Suppressing the subscripts, let $\phi(x)$ and $\beta(x)$ represent positions of the final wavefront and waveback to traverse the entire fiber left-to-right, prior to the initiation of a right-to-left propagating action potential (see Fig. 3). For convenience, let $t = 0$ correspond to the firing time of the $x = 0$ pacemaker, so that $\phi(0) = 0$. Then ϕ satisfies a trivial initial value problem:

$$\frac{d\phi}{dx} = \frac{1}{c(D^*)}, \quad \phi(0) = 0 \qquad \Rightarrow \qquad \phi(x) = \frac{x}{c(D^*)}. \tag{6}$$

It follows that

$$\beta(x) = \phi(x) + f(D^*) = \frac{x}{c(D^*)} + f(D^*). \tag{7}$$

The vulnerable window for triggering a right-to-left propagating action potential begins (approximately) at time $\beta(L) = f(D^*) + L/c(D^*)$, when the final left-to-right waveback reaches the distal end of the fiber. The vulnerable window ends at time $B + \phi(L) = B + L/c(D^*)$, the time at which a subsequent left-to-right wavefront (triggered by the firing of the $x = 0$ pacemaker at time $t = B$) is due to reach the distal boundary.

Depending on B and the firing time of the distal pacemaker during the vulnerable window, the resulting right-to-left action potential may either block a left-to-right action potential in the middle of the fiber [Fig. 3(a)] or traverse the entire fiber uninterrupted [Fig. 3(b)]. In order for the latter to occur, the right-to-left propagating wavefront must arrive at the $x = 0$ boundary by time $t = B$. To derive conditions for this, let us establish the following notation:

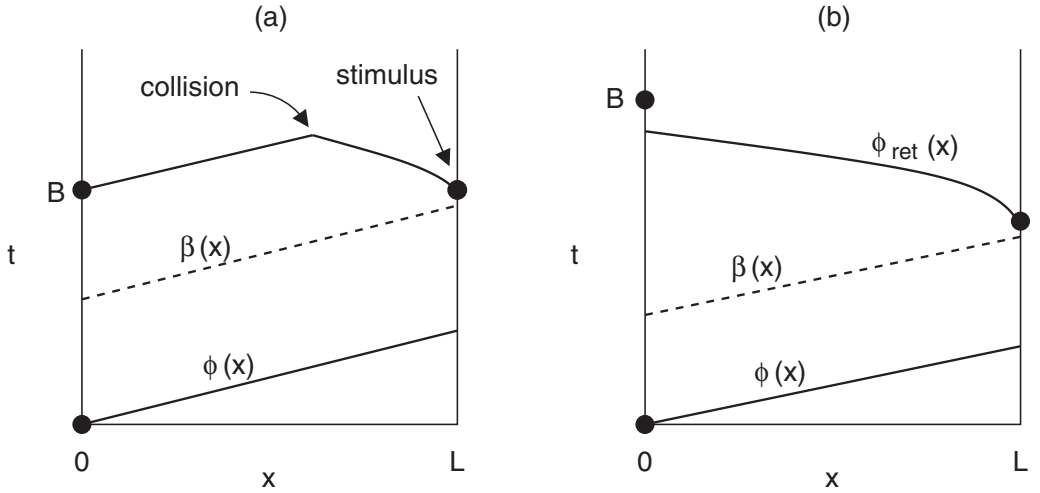

FIG. 3. Initiation of retrograde propagation due to firing of a distal pacemaker during a vulnerable time window. (a) The right-to-left propagating action potential collides with a subsequent left-to-right action potential in the middle of the fiber. (b) The right-to-left propagating action potential traverses the entire fiber unblocked.

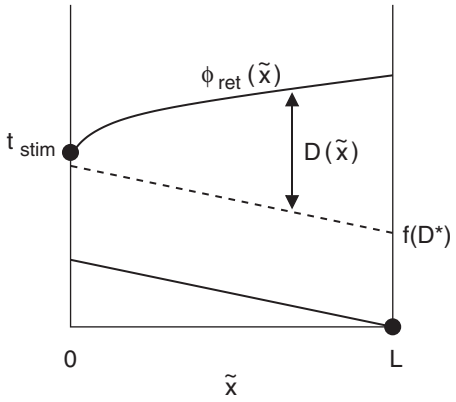

FIG. 4. Schematic of a retrograde action potential that interrupts a steady train of (nonretrograde) action potentials.

(i) $\tilde{x} = L - x$ is distance from the distal pacemaker boundary.

(ii) t_{stim} is the time at which the stimulus at $\tilde{x} = 0$ elicits a propagating action potential.

(iii) ϕ_{ret} denotes the position of the wavefront of the retrograde action potential. See Figs. 2(b) and 4.

(iv) $D(\tilde{x}) = \phi_{\text{ret}}(\tilde{x}) - \beta(\tilde{x})$ is the diastolic interval preceding the arrival of the retrograde wavefront. See also Eq. (7) and Fig. 4.

Then $D(\tilde{x})$ satisfies an initial value problem

$$\frac{dD(\tilde{x})}{d\tilde{x}} = \frac{1}{c(D(\tilde{x}))} + \frac{1}{c(D^*)},$$
$$D(0) = t_{\text{stim}} - \left[\frac{L}{c(D^*)} + f(D^*)\right]. \tag{8}$$

Setting $\tilde{x} = L$ in the equation $D(\tilde{x}) = \phi_{\text{ret}}(\tilde{x}) - \beta(\tilde{x})$, we find that

$$\phi_{\text{ret}}(\tilde{x})\Big|_{\tilde{x}=L} = t_{\text{stim}} + \int_0^L \frac{1}{c(D(y))} dy.$$

Thus, the retrograde action potential will traverse the fiber uninterrupted if

$$t_{\text{stim}} + \int_0^L \frac{1}{c(D(y))}\, dy < B. \tag{9}$$

Of course, applying the inequality (9) requires solution of the (typically nonlinear) initial value problem (8). An alternate, more intuitive way of stating Condition (9) is via the inequality

$$f(D^*) + D(L) < B, \tag{10}$$

where $D(L)$ is obtained through solving the initial value problem (8). See also Fig. 4, specifically the behavior at the $\tilde{x} = L$ boundary.

III. RESULTS AND NUMERICAL SIMULATIONS

We performed numerical simulations of the two-current model of equations (1) and (2), experimenting with various mechanisms for reversals. A movie illustrating the reversal phenomenon is provided in the supplemental material [15]. The movie was generated using the parameters in the second row of Table I and using the pacing protocol described in Sec. III B 1 ($B = 550$ ms, $A = 200$ ms, $\delta = 0.1$, and $P = 60\,000$ ms). After a brief initial transient, a sustained pattern of right-to-left propagation is established, with occasional interruptions due to collisions between APs propagating in opposite directions. Approximately 1 min, 10 s into the video, slowdown of the right pacemaker allows the left pacemaker to establish sustained left-to-right propagation during the next minute of the video. Approximately 2 min, 13 s into the video, slowdown of the left pacemaker enables another reversal—after a brief transient, right-to-left propagation resumes.

Note that in generating this movie, we opted to use model parameters typical of mammalian APs as opposed to tunicate APs. As explained in the next subsection, mammals have substantially shorter APD and faster CV than tunicates, making it easier to see the waveforms of propagating APs in movies. Rather than providing movies of simulated tunicate APs, we find it more instructive to examine space-time plots of wavefronts and wavebacks as in all upcoming figures.

A. Parameters

Tunicates and mammals can have an order-of-magnitude difference both in APD and in CV [13], and in the firing rates of their pacemaker cells [14]. In low-temperature environments, tunicate APD may exceed 2 s, whereas 200 ms would be more typical for human APD. A typical tunicate CV might be 2 cm/s, easily 20–40 times slower than human ventricular CV. In some experiments [14], average firing rates of tunicate pacemakers were measured as 17 beats per minute at 15°C, considerably slower than what one observes in most (nonhibernating) mammals. With these data in mind, equations (3) and (4) allow us to propose tunicate-specific values of the parameters appearing in the two-current model equations (1) and (2). The following observations are important:

(i) the maximum values of APD and CV may be obtained by taking the limit of large DI in Eqs. (3) and (4);

(ii) increasing τ_{in} reduces the maximum values of both APD and CV, whereas increasing τ_{out} increases the maximum values of both APD and CV;

(iii) varying τ_{open} has no effect on the maximum values of APD and CV, but sets the time scale over which the APD and CV restitution functions reach their plateaus;

(iv) increasing τ_{close} increases the maximum APD, but has no effect on the maximum CV;

TABLE I. Reference parameter sets used in our numerical simulations with the two-current model Eqs. (1)–(2).

	τ_{in} (ms)	τ_{out} (ms)	τ_{open} (ms)	τ_{close} (ms)	κ (cm^2/ms)	v_{crit} (dimensionless)
Tunicate	0.3	3.0	200	1300	10^{-5}	0.13
Mammal	0.1	2.4	130	150	10^{-3}	0.13

(v) CV is proportional to $\sqrt{\kappa}$, but κ has no effect on APD; and

(vi) in order for a cell to be able to produce an action potential, it is necessary that $h_{\min} = 4\tau_{\text{in}}/\tau_{\text{out}}$ be suitably small; see Ref. [22] for details. Moreover, Eqs. (3) and (4) are derived using asymptotic methods under the presumption that $\epsilon = \tau_{\text{out}}/\tau_{\text{close}}$ is small.

Bearing these considerations in mind, we propose the parameters appearing in the first row of Table I as reference parameters for models of tunicate cardiac action potentials. For those parameters, Eqs. (3) and (4) predict a maximum APD of 1244 ms and a maximum CV of 2.70 cm/s.

Because tunicates exhibit such long APD and short CV, numerical simulations of their action potential reversals can be time consuming. For this reason, we have identified a second set of reference parameters (second row of Table I) which we use in many of our numerical explorations of the reversal phenomenon. This second set of parameters leads to APD and CV akin to what one might expect in mammals—Eqs. (3) and (4) predict a maximum APD of 291 ms and a maximum CV of 61.4 cm/s.

B. Numerical simulations of tunicate action potentials

Here we explore two mechanisms for reversals: out-of-phase, periodic fluctuations in the firing rates of both pacemakers and reversals due to stochastic variability the firing rates of two pacemakers with the same mean firing rate. We also offer numerical evidence of the predictive power of the reversal criteria in Sec. II E. Almost all of our simuluations used pacing protocols for which every stimulus elicited a propagating action potential. As we mention in Sec. III B 4, it is important to note that rapid pacing can lead to behaviors such as spatially discordant alternans and conduction block.

1. Periodic fluctuations in firing rates of both pacemakers

Slow, out-of-phase variations in the interstimulus intervals of both pacemakers can lead to reversals rather easily. This is reminiscent of the "pacemaker fatigue" scenario described in Ref. [10]. To illustrate this phenomenon, we solved the two-current model equations (1) and (2) numerically on a one-dimensional domain of length $L = 3.0$ cm using a forward Euler method with $\Delta x = 0.01$ cm and $\Delta t = 0.02$ ms. No-flux boundary conditions were enforced at both ends of the fiber. Stimuli were applied at both ends of the fiber with stimulus strength approximately 3 times the threshold needed to elicit a propagating action potential in a quiescent fiber. At time $t = 0$, a stimulus was applied at the left ($x = 0$) pacemaker, eliciting a left-to-right propagating AP. For $t > 0$, interstimulus intervals for the left and right pacemaker cells varied according to smoothed, periodic square-wave functions of opposite phase:

$$S_l(t) = B + \frac{A \arctan(\sin(2\pi t/P)/\delta)}{\arctan(1/\delta)} \text{ (left pacemaker)},$$

$$S_r(t) = B - \frac{A \arctan(\sin(2\pi t/P)/\delta)}{\arctan(1/\delta)} \text{ (right pacemaker)}.$$

Here B denotes the mean interstimulus interval, A and P denote the amplitude and period of variation in interstimulus intervals, and the parameter δ adjusts the abruptness of the transitions between fast and slow pacing (approximately square wave as $\delta \to 0$ and nearly sinusoidal for large δ). Figure 5(b) illustrates the variation of interstimulus intervals for $B = 2000$ ms, $A = 500$ ms, $P = 60\,000$ ms, and $\delta = 0.1$.

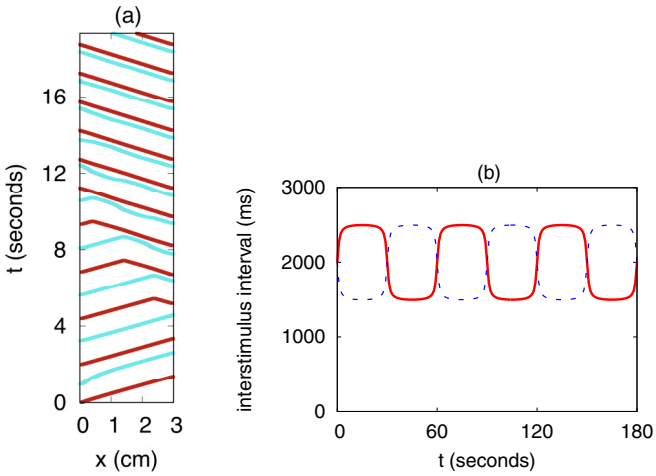

FIG. 5. (a) Space-time plot of wavefronts (dark red) and wavebacks (light blue) of action potentials in simulations of tunicate heart tissue. After two beats of left-to-right propagation, there are three collisions between action potentials propagating in opposite directions before a pattern of right-to-left propagation is established. (b) Interstimulus intervals for the left pacemaker (solid red curve) and the right pacemaker (dashed blue curve). See text for details.

Figure 5(a) shows results of numerical simulations of (1) and (2) using the parameters in the first row of Table I and the pacing protocol described in the preceding paragraph. The first 20 s of pacing are shown. After two left-to-right propagating APs traverse the fiber, there are three collisions between APs propagating in opposition directions before a pattern of right-to-left propagation is established. This behavior is reasonable given the pacing protocol: Initially, both pacemakers have interstimulus intervals of approximately $B = 2000$ ms but decreasing to 1500 ms at the right pacemaker and increasing to 2500 ms at the left pacemaker. Hence, the right pacemaker overdrives the left pacemaker and establishes sustained right-to-left propagation. Continuing the simulation further in time (not shown), the system sustains a pattern of 15–16 beats of unidirectional propagation, 2–3 beats in which collisions of action potentials occur within the interior of the fiber, 15–16 beats of unidirectional propagation in the opposite direction.

2. Random variations in firing rates of both pacemakers

Cardiac pacemakers may exhibit considerable variability in interstimulus intervals, due to fluctuations in neurotransmitters such as acetylcholine and norepinephrine which regulate the firing rates. Clinically, interstimulus intervals are identified with RR intervals in electrocardiogram (ECG) recordings. Data from short-term (i.e., several minutes) ECG recordings in humans suggest that standard deviations of interstimulus are roughly 10% as large as the mean interstimulus intervals [23]. Assuming that tunicates exhibit a similar degree of heart rate variability, we explore the role of such variability in

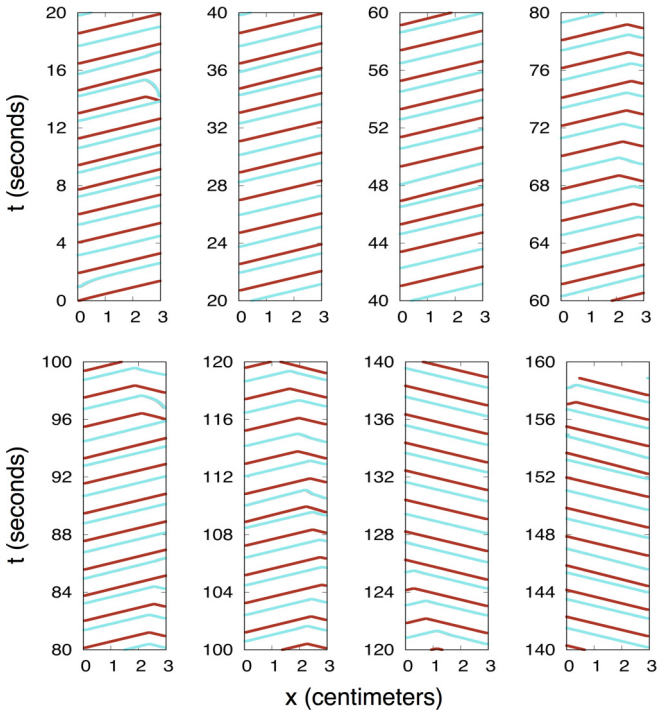

FIG. 6. Space-time plot of wavefronts (dark red) and wavebacks (light blue) of action potentials in simulations of tunicate heart tissue, presuming that the two pacemakers have the same mean interstimulus interval (2000 ms) and same standard deviation (200 ms). See text for details.

eliciting reversals of propagation. To this end, we performed numerical simulations of (1) and (2) using the parameters in the first row of Table I, but with a different pacing protocol: The interstimulus intervals for both pacemakers had the same mean and with the same amount of Gaussian noise affecting the stimulus times. More precisely, after initiating left-to-right propagation by stimulating at $x = 0$ when $t = 0$, each pacemaker's subsequent firing time was chosen according to the rule

$$\text{next stimulus time} = \text{previous stimulus time} + B + \text{noise},$$

where $B = 2000$ ms, and the noise was normally distributed with mean 0 and standard deviation $\sigma = 200$ ms. Choosing σ to be 10% as large as B reflects our previous remarks regarding heart rate variability.

Figure 6 shows sample results of these numerical simulations. During the first 62 s, there is a steady pattern of left-to-right propagation. Between $t = 64$ s and $t = 84$ s, action potentials propagating in opposite directions collide within the interior of the fiber. Left-to-right propagation is restored for several beats ($84 < t < 96$), before another cluster of collisions ($96 < t < 124$). Finally, sustained right-to-left propagation is established beyond $t = 124$ s. These simulations suggest that stochastic variability of pacemaker firing rates can, by itself, lead to reversals of propagation, even if both pacemakers have the same mean interstimulus interval. However, Fig. 6 is not completely consistent with experimental observations of reversals in tunicate hearts. The figure suggests that many collisions may occur within the interior of the domain, for tens of seconds before one pacemaker emerges as dominant. Collisions occur during time windows in which the two pacemakers are nearly in-phase with one another. In order for one pacemaker to establish dominance, it must experience a "lucky streak" of overdriving the competing pacemaker for several beats in a row (or at least the vast majority of beats within a given time window). This is the sort of behavior shown in the interval $108 < t < 124$ in Fig. 6.

3. Validating the analytical criteria for reversals

Further numerical simulations confirm that Eqs. (7) and (9) provide accurate information regarding whether reversals can occur. To this end, we performed numerical simulations of (1) and (2) with the parameter choices appearing in the first row of Table I, using the pacing protocol mentioned in Sec. II E. The left pacemaker fired periodically with period B, without interference from the right pacemaker, until approximate steady-state was achieved. Then, a single stimulus was applied at the right pacemaker, near the beginning of the vulnerable window for initiation of retrograde propagation.

Figure 7(a) shows the results of applying this pacing protocol in a fiber of length $L = 3.0$ cm with period $B = 2000$ ms. The asymptotic formulas (3) and (4) predict that, for this B, the steady-state values of APD, DI, and CV are 1227 ms, 773 ms, and 2.665 cm/s (respectively), predicting that each action potential in the wave train should require 1126 ms to traverse the fiber. Let $t = 0$ correspond to the final time at which the the left pacemaker fires prior to the firing of the right pacemaker. Substituting $D^* = 773$ ms into Eqs. (6) and (7), the above asymptotic approximations predict that the wavefront and waveback of the resulting action potential will arrive at the far end of the fiber at times $\phi(3.0) = 1126$ ms and $\beta(3.0) = 1126 + 1227 = 2353$ ms. Thus, a vulnerable window for triggering right-to-left propagation is expected to start at $t \approx 2353$ ms. These numbers are remarkably close to those observed in numerical simulations of the PDE model, using a forward Euler solver with $\Delta t = 0.01$ ms and $\Delta x = 0.0025$ cm. In the PDE model simulations, the steady-state values of APD and DI were 1223 and 777 ms, and the time required for the left-to-right APs to traverse the fiber was 1123 ms. By firing the right pacemaker at time $t = 2400$ ms (see figure), a right-to-left propagating AP was generated. Despite the fact that this AP was generated very early within the vulnerable window, a collision with a left-to-right AP still occurred ($t \approx 2.08$ s, $x \approx 2.1$ cm). For this particular B and fiber length L, it is impossible to completely reverse the direction of propagation with a single stimulus, no matter how early in the vulnerable window such a stimulus is applied.

In order to accomplish a reversal of propagation using a single, well-timed stimulus of the right pacemaker, we repeated these simulations with a shorter fiber ($L = 2.0$ cm) and a longer B for the left pacemaker ($B = 3000$ ms). The results are shown in Fig. 7(b). The asymptotic formulas (3) and (4) predict that, for this B, the steady-state values of APD, DI, and CV are 1244 ms, 1756 ms, and 2.702 cm/s (respectively), suggesting that each AP in the wave train should require 740 ms to traverse the fiber. Substituting $D^* = 1756$ ms into Equations (6) and (7), this time the asymptotic approximations predict that the wavefront and waveback of

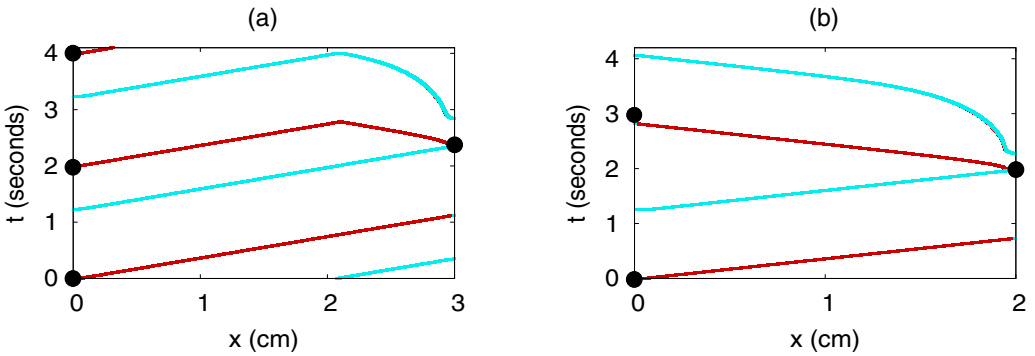

FIG. 7. Space-time plots of wavefronts (dark red) and wavebacks (light blue) of action potentials in simulations of tunicate heart tissue, assuming that the left pacemaker fires periodically and the right pacemaker fires a single stimulus during the vulnerable time window. Stimuli are indicated by bold dots. (a) A collision of action potentials on the interior of the fiber. (b) Establishment of retrograde propagation via a single, well-timed stimulus of the right pacemaker. See text for details.

the resulting action potential will arrive at the far end of the fiber at times $\phi(2.0) = 740$ ms and $\beta(2.0) = 740 + 1244 = 1984$ ms. Thus, a vulnerable window for triggering right-to-left propagation is expected to start at $t \approx 1984$ ms. As before, there is excellent (less than 1% relative error) agreement between the times $\phi(2.0)$ and $\beta(2.0)$ predicted by asymptotics and the times obtained by numerical simulations of the PDE model. By firing the right pacemaker at $t = 2000$ ms (i.e., almost immediately after the predicted start of a vulnerable window), a right-to-left propagating AP was generated. This AP traversed the entire fiber, reaching the $x = 0$ boundary at time $t = 2820$ ms, shortly before the left pacemaker was due to fire at $t = 3000$ ms. Because cells in the vicinity of the left pacemaker had not recovered excitability by $t = 3000$ ms, a left-to-right propagating AP was not generated.

4. Discordant alternans and conduction block

Until now, we have considered pacing protocols for which every stimulus elicited a propagating action potential. Pacing was sufficiently slow that little spatial variation in DI, APD, and CV occurred, making it easier for us to study reversals by establishing the sorts of scenarios depicted in Fig. 3. By contrast, rapid pacing can introduce spatial heterogeneity of DI, APD, and CV, and very rapid pacing can lead to conduction block due to the fact that cardiac cells present refractoriness. Figure 8 illustrates the sorts of dynamical behaviors that one might observe of one of the pacemakers fires rapidly. Figure 8(a) was generated using precisely the same pacing protocol as in Fig. 5(a) but with τ_{close} increased to 1500 ms so as to increase APD. Following an initial transient of several beats, a pattern of right-to-left propagation is established with considerable spatial variation in DI. The fiber exhibits *spatially discordant alternans*: beat-to-beat alternation of APD in which some cells alternate short-long while others alternate long-short. Figure 8(b) was generated using a very different protocol. Starting at $t = 0$, an initially quiescent fiber was paced with period 2000 ms at $x = 0$ and with period 1250 ms at $x = 3$. Parameters were taken from the first row of Table I but with $\tau_{\text{close}} = 1500$ ms. After a collision in the middle of the fiber, the stimuli applied to the right boundary at $t = 1250$ ms and $t = 2500$ ms successfully generate right-to-left propagating APs. Due to restitution of CV, these APs slow down as the wavefronts closely follow wavebacks of preceding APs, establishing considerable heterogeneity along the fiber. Half of the remaining stimuli applied at the $x = 3$ end of the fiber (stimulus times indicated by arrows in the figure) fail to elicit APs, because the cells have yet to recover excitability when those stimuli are applied. A 2:1 stimulus:response pattern is established at the $x = 3$ boundary, and the arrows in the figure indicate which stimuli are ignored. This effectively doubles the pacing period at $x = 3$ to 2500 ms, allowing the $x = 0$ pacemaker to overdrive the $x = 3$ pacemaker and establishing left-to-right propagation after roughly 16 s.

C. General observations

Figure 7 helps illustrate some rather intuitive observations regarding favorable conditions for reversals. Reversals require a careful interplay among APD, CV, the fiber length L, and

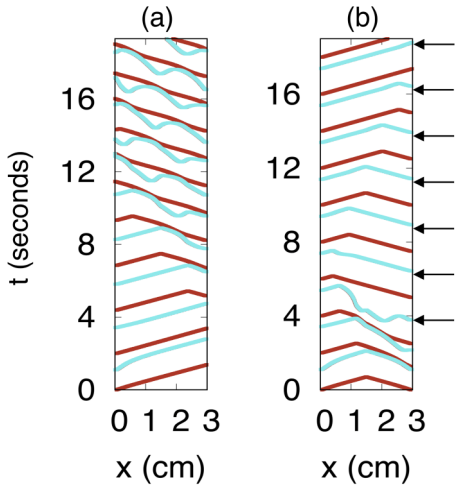

FIG. 8. (a) Changing τ_{close} to 1500 ms and repeating the simulations used to generate Fig. 5(a), discordant alternans occurs after a brief initial transient. (b) Periodic stimulation of the $x = 0$ boundary with period 2000 ms and the $x = 3$ boundary with period 1250 ms can lead to a pattern of 2:1 conduction block. Arrows indicate times at which stimulating the $x = 3$ boundary failed to elicit a propagating action potential.

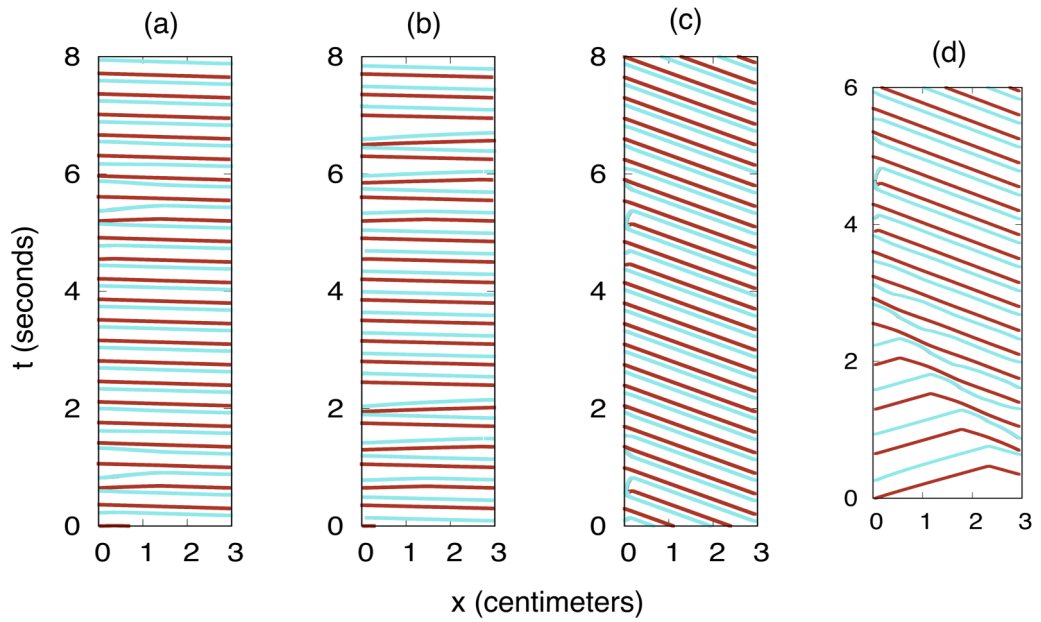

FIG. 9. Space-time plot of wavefronts (dark, red) and wavebacks (light, blue) of simulated APs in a fiber of length $L = 3.0$ cm. The $x = 0$ end of the fiber was paced with constant period 650 ms while the $x = 3$ end of the fiber was paced with constant period 350 ms. (a) Steady-state response using the parameters in the second row of Table I. (b) Same as in (a) but with τ_{close} reduced to 75 ms. (c) Same as in (a) except that $\kappa = 10^{-5}$. (d) Same parameters as in (c), showing the initial transient response if the $x = 3$ pacemaker had been turned off prior to time $t = 0$. See text for details.

the firing rates of both pacemakers. Here are some concrete observations:

(i) Small L tends to favor unidirectional propagation, because each AP is more likely to traverse the fiber without colliding with an AP propagating in the opposite direction. Large L increases the likelihood of collisions between APs traveling in opposite directions.

(ii) When two pacemakers fire with vastly different mean interstimulus intervals, there is increased likelihood of establishing unidirectional propagation from the faster pacemaker toward the slower pacemaker.

(iii) Equations (3) and (4) and the remarks in Sec. III A elucidate the roles of the two-current model parameters in promoting reversals and/or collisions of APs within the interior of the spatial domain. Figure 9(a) illustrates the steady-state response obtained by simulating the two-current model in a fiber of length $L = 3.0$ cm paced periodically at both ends (period 350 ms at $x = 0$ and period 650 ms at $x = 3.0$). A sustained pattern of right-to-left propagation is established, with an occasional collision whenever the $x = 0$ pacemaker supplies a stimulus during a vulnerable window (approximately once every 4 s). As illustrated in Fig. 9(b), reducing τ_{close} to 75 ms promotes additional collisions. This makes sense intuitively—reducing τ_{close} reduces APD but not CV. The reduction in APD lengthens the vulnerable time windows, enabling more stimuli at $x = 0$ to elicit left-to-right propagation. Figure 9(c) was generated using the same parameters as Fig. 9(a), but with the diffusion coefficient κ reduced to 10^{-5}. Reduced κ has no effect on APD, but reduces CV. By reducing CV while maintaining rapid pacing at the $x = 3$ end of the fiber, stimuli supplied at $x = 0$ cannot generate left-to-right propagating APs which make substantial progress before being blocked by a right-to-left AP. Figure 9(d) illustrates the initial transient obtained using the same parameters as Fig. 9(c) but with the $x = 3$ pacemaker turned off prior to time $t = 0$. Due to the slow CV, there is a prolonged transient (5 beats) required for the $x = 3$ pacemaker to establish sustained right-to-left propagation.

Given a more physiologically detailed ionic model of the cardiac action potential, one might undertake a more comprehensive survey of how key parameters affect likelihood of reversals and collisions.

IV. DISCUSSION

In this article, we have proposed a model for heart reversals in tunicates, using previously published data to estimate model parameters. Using asymptotic approximations for APD and CV restitution functions [Eqs. (3) and (4)], we derived criteria for initiating retrograde propagation and/or triggering a reversal via a single stimulus within the vulnerable time window [Eqs. (7) and 9)]. Equipped with these restitution functions and reversal criteria, it is easy to identify heart lengths L and pacing protocols that generate reversals. Because the restitution functions are derived from an ionic model, one may explore the roles played by various physiological parameters (such as τ_{in}, a time constant loosely associated with the fast sodium current) in promoting or inhibiting reversals. Numerical simulations of gradual pacemaker variability, as illustrated in Fig. 5, produce dynamical behavior similar to that observed experimentally (see also the next paragraph). Notably, our numerical simulations also suggest that variability of pacemaker firing rates may elicit reversals (Fig. 6), even if both pacemakers have the same mean interstimulus interval. However, it is unlikely that such variability alone could be the primary mechanism for reversals.

Otherwise, our model would suggest that many collisions of APs might occur whenever the pacemakers are approximately in-phase with one another. This may lead to prolonged time windows (tens of seconds) during which neither pacemaker is able to establish dominance, thereby preventing the heart from effectively pumping. It seems plausible that tunicates experience some hybrid of (i) gradual drift of pacemaker firing rates and (ii) stochastic heart rate variability, and that the former is the primary contributor to reversals.

Our mathematical model captures key phenomena appearing in our experimentally obtained video (see the supplemental material [15]). In that video, there are reversals at times 00:10, 02:20, and 02:50. During the 15 s leading up to the reversal at 02:50, the period of the pacemaker driving bottom-to-top propagation is substantially longer than the period of the pacemaker driving top-to-bottom propagation during the 15 s following the reversal. Regarding collisions, there seem to be some times (e.g., at times 02:01 and 02:04) at which two advancing wavefronts clearly collide and annihilate one another. However, it is difficult to distinguish between actual wavefronts (those due to advancing electrical waves) and "illusory" wavefronts due to mechanical deformation of the heart as it relaxes after blood is pumped. For example, throughout the second full minute of video, top-to-bottom contraction is sustained. As each downward propagating wavefront reaches the bottom half of the heart, there is the appearance of what looks like a much smaller upward propagating wavefront in the top half of the heart. We believe that this is illusory in the sense that it is a consequence of mechanical relaxation of the heart muscle, and has nothing to do with electrical activity. We also mention that we cannot rule out the possibility that the heterogeneity of the heart muscle tissue and the three-dimensional structure of a real heart could allow two APs propagating in opposite directions to find conduction pathways enabling them to pass around one another, though we find it highly unlikely that such behavior could occur in a normal, appropriately large heart.

While tunicates are fascinating creatures in their own right, one might wonder about the broader importance of understanding their heart behavior. Tunicates are sometimes regarded as model organisms for understanding heart development in vertebrates: as they are vertebrates' closest invertebrate relatives [24], it is believed that aspects of embryonic heart development in vertebrates can be understood using tunicates as a proxy [1]. There are still more compelling reasons to understand the dynamics of multiple pacemaker sites. Ectopic automaticity foci in human hearts can cause various types of arrhythmia depending on their location within the heart. Competition between the sinus node (the heart's natural pacemaker, an automaticity focus located in the right atrium) and ectopic foci can cause intermittent transitions from normal rhythm to arrhythmia.

Given additional resources for experimentation, there are several areas of further study that we would propose. Here we have idealized the tunicate heart as a homogeneous, one-dimensional excitable medium. A more refined model might incorporate tissue heterogeneity and a more accurate description of tunicate heart geometry. The two-current model of the membrane potential offers a major advantage in that it lends itself to asymptotic derivation of restitution functions; however, it lacks the level of detail necessary for postulating physiological bases for reversals. Asymptotic approximations for APD restitution functions are available for more physiologically detailed three-current models [25–27]. More detailed models of the action potential (see Ref. [28], for instance) might offer insights regarding the ionic basis for reversals. Although asymptotic formulas for APD and CV are not available for such models, straightforward numerical solution of the differential equations allows one to explore the effects of model parameters on APD and CV. Given the resources to perform additional experiments with adult tunicates, we hope to complete a careful exploration of pacemaker firing rates and heart rate variability in adult tunicates.

[1] P. Lemaire, Development **138**, 2143 (2011).

[2] J. Xavier-Neto, B. Davidson, M. Simoes-Costa, H. Castillo, A. Sampaio, and A. Azambuja, in *Heart Development and Regeneration*, 1st ed., edited by N. Rosenthal and R. Harvey (Elsevier Science and Technology, London, 2010), Vol. 1, pp. 3–38.

[3] A. Santhanakrishnan and L. Miller, Cell Biochem. Biophys. **61**, 1 (2011).

[4] B. McMahon, Comparative evolution and design in non-vertebrate cardiovascular systems, *Ontogeny and Phylogeny of the Vertebrate Heart* (Springer, New York, 2012), pp. 1–33.

[5] M. Kalk, Tissue and Cell **2**, 99 (1970).

[6] M. Anderson, J. Exp. Biol. **49**, 363 (1968).

[7] A. C. Heron, J. Mar. Biol. Assoc. UK **55**, 959 (1975).

[8] C. A. Haywood and H. P. Moon, J. Exp. Biol. **27**, 14 (1950).

[9] C. A. Haywood and H. P. Moon, Nature **172**, 40 (1953).

[10] B. J. Krijgsman, Biol. Rev. **31**, 288 (1956).

[11] C. C. Mitchell and D. G. Schaeffer, Bull. Math. Biol. **65**, 767 (2003).

[12] N. F. Otani, Phys. Rev. E **75**, 021910 (2007).

[13] M. E. Kriebel, J. General Physiol. **50**, 2097 (1967).

[14] M. E. Kriebel, Biol. Bull. **134**, 434 (1968).

[15] See Supplemental Material at http://link.aps.org/supplemental/10.1103/PhysRevE.102.062421 for a movie of experimentally recorded reversals as described at the start of Sec. II and for a movie of simulated reversals as described at the start of Sec. III.

[16] L. D. Waldrop and L. A. Miller, J. Exp. Biol. **218**, 2753 (2015).

[17] J. W. Cain and D. G. Schaeffer, SIAM Rev. **48**, 537 (2006).

[18] J. W. Cain, E. G. Tolkacheva, D. G. Schaeffer, and D. J. Gauthier, Phys. Rev. E **70**, 061906 (2004).

[19] Stimuli fail to elicit action potentials in cells that have not recovered excitability following a prior excitation.

[20] For a discussion of when this is justified, see Ref. [18].

[21] G. M. Hall, S. Bahar, and D. J. Gauthier, Phys. Rev. Lett. **82**, 2995 (1999).

[22] M. Beck, C. K. R. T. Jones, D. G. Schaeffer, and M. Wechselberger, SIAM J. Appl. Dyn. Syst. **7**, 1558 (2008).
[23] L. A. Lipsitz, J. Mietus, G. B. Moody, and A. L. Goldberger, Circulation **81**, 1803 (1990).
[24] F. Delsuc, H. Brinkmann, D. Chourrout, and H. Phillippe, Nature **439**, 965 (2006).
[25] F. Fenton and A. Karma, Chaos **8**, 20 (1998).
[26] E. G. Tolkacheva, D. G. Schaeffer, D. J. Gauthier, and C. Mitchell, Chaos **12**, 1034 (2002).
[27] D. G. Schaeffer, J. W. Cain, D. J. Gauthier, S. S. Kalb, R. A. Oliver, E. G. Tolkacheva, W. Ying, and W. Krassowska, Bull. Math. Biol. **69**, 459 (2007).
[28] C. H. Luo and Y. Rudy, Circ. Res. **74**, 1071 (1994).